Available online at www.sciencedirect.com
SCIENCE DIRECT®
Earth and Planetary Science Letters 221 (2004) 409–419
EPSL
www.elsevier.com/locate/epsl

Axial vs. equatorial dipolar dynamo models with implications for planetary magnetic fields

Julien Aubert *, Johannes Wicht

Max-Planck-Institute for Aeronomy, Max-Planck-Strasse 2, 37191 Katlenburg-Lindau, Germany

Received 3 July 2003; received in revised form 27 January 2004; accepted 29 January 2004

Abstract

We present several numerical simulations of a self-consistent dynamo model in a rotating spherical shell. The solutions have two different field configurations. Besides magnetic fields dominated by the axial dipole component, we also find configurations where a dipole in the equatorial plane is the dominating component. Both types are stable in a parameter regime of intermediate shell thickness and Rayleigh numbers close to onset of convection. Axial dipole solutions are subcritical in all the simulations explored while the equatorial dipole cases are supercritical at low Rayleigh numbers but become metastable at higher Rayleigh numbers. The magnetic field strength saturates at a much lower amplitude for the equatorial dipole dynamos, and the Elsasser number is significantly smaller than in the axial configuration. The reason is that the mainly horizontal field in the equatorial dipole solution is incompatible with the motion of convective cyclones and anticyclones. The axial dipole field, on the other hand, is predominantly aligned with the axis of anticyclones, only cyclones are disrupted by horizontal field lines passing through. This configuration can therefore accomodate stronger convective flows and, consequently, is the only one remaining stable at higher Rayleigh numbers. These arguments should pertain in all planetary dynamos that are governed by strong rotational constraints. They offer an explanation why the Elsasser numbers inferred for Uranus and Neptune are much lower than the Elsasser numbers of Jupiter, Saturn, and Earth.

Keywords: numerical dynamo simulation; axial dipole; equatorial dipole; Uranus; Neptune; magnetic field

1. Introduction

Before the spacecraft Voyager II visited Uranus and Neptune it was consensus that planetary magnetic fields are dominated by a dipole aligned with the planetary rotation axis. The magnetic fields of the Earth, Saturn, Jupiter, and probably also Mercury, fall into this category. But the magnetic fields of Uranus and Neptune are different. Their dipole axes are tilted at 50° and 47°, respectively, to the planetary spin axis. Global field models also show that both planetary magnetic fields have significant quadrupole and octupole contributions [1], much larger than, for example, in the geomagnetic field.

Kinematic dynamo calculations have demonstrated that axial dipole configurations are more

* Corresponding author. Tel.: +49-5556-9790; Fax: +49-5556-979-240.
E-mail address: jaubert@gwdg.de (J. Aubert).

0012-821X/04/$ – see front matter © 2004 Elsevier B.V. All rights reserved.
doi:10.1016/S0012-821X(04)00102-5

frequent. Some of the tested flows nevertheless favor equatorial dipole solutions [1,2]. Likewise, the magnetic field measured in the Karlsruhe dynamo experiment [3] is equivalent to a dipole lying in the equatorial plane. Most of the self-consistent dynamo simulations, on the other hand, are geared to model the geodynamo and feature solutions dominated by an axial dipole [4–6]. The equatorial dipole contribution may only dominate in a transient state during a reversal. An exception is the self-consistent simulation by Ishihara and Kida [7]. They find a persisting equatorial dipole solution at a critical Rayleigh number close to onset of convection. However, when they double the Rayleigh number the solution switches to an axial dipole dominated configuration.

Here, we present a region of the parameter space where dynamos of both configurations can coexist. We highlight important differences in the respective dynamo mechanisms and discuss our results within the scope of planetary applications. For simplicity we will refer to axial and equatorial dipole solutions for magnetic fields which are dominated by the respective dipole component. All solutions presented here also contain higher field harmonics in addition to the dipole. Axial and equatorial dipoles are representatives of two different symmetry classes. The axial dipole field is antisymmetric with respect to the equator while the equatorial dipole field is symmetric. Confusingly, these two classes are sometimes referred to as dipole and quadrupole dynamos, because axisymmetric fields are thought to be the dominant contributions in both symmetry classes. Grote et al. [8] have explored the parameter space for the existence of dipolar and quadrupolar dynamos. Contrary to the results presented here, their solutions are always dominated by axisymmetric components.

2. Numerical model

We study the dynamo action in an electrically conducting, thermally convecting Boussinesq fluid. The fluid is contained in a spherical shell that rotates about the z-axis with rotation rate Ω. We formulate a dimensionless model and use the shell thickness, i.e. the difference between inner and outer shell radii r_i and r_e, as a length scale. The magnetic diffusion time D^2/η serves as the time scale, and the Elsasser number $(\rho\mu\eta\Omega)^{1/2}$ scales magnetic induction $\mathbf{B}$. Here, η is the magnetic diffusivity of the fluid, ρ is the fluid density, and μ the magnetic permeability.

The boundaries are isothermal and the difference between inner and outer boundary temperature, T_i and T_o, respectively, is used as the temperature scale. The dimensionless equation system includes the Navier–Stokes equation, the dynamo equation, the heat equation, the simplified continuity equation, and the condition that magnetic induction is divergence free:

$$\frac{E}{qPr}\left(\frac{\partial \mathbf{u}}{\partial t}+\mathbf{u}\cdot\nabla\mathbf{u}\right)+2\mathbf{e}_z\times\mathbf{u}= -\nabla\Pi+Ra\,q\,Pr\,\frac{r}{r_e}\mathbf{e}_r T+(\nabla\times\mathbf{B})\times\mathbf{B}+E\nabla^2\mathbf{u} \quad (1)$$

$$\frac{\mathrm{d}\mathbf{B}}{\mathrm{d}t}=\nabla\times(\mathbf{u}\times\mathbf{B})+\nabla^2\mathbf{B} \quad (2)$$

$$\frac{\partial T}{\partial t}+\mathbf{u}\cdot\nabla T=q\nabla^2 T \quad (3)$$

$$\nabla\cdot\mathbf{u}=0. \quad (4)$$

$$\nabla\cdot\mathbf{B}=0 \quad (5)$$

The non-dimensional control parameters are the Rayleigh number Ra, the Ekman number E, the Prandtl number Pr, the Roberts number q, and the radius ratio γ:

$$Ra=\frac{\alpha g_o \Delta T D}{\nu\Omega} \quad (6)$$

$$E=\frac{\nu}{\Omega D^2} \quad (7)$$

$$Pr=\frac{\nu}{\kappa} \quad (8)$$

$$q=\frac{\kappa}{\eta} \quad (9)$$

$$\gamma=\frac{r_i}{r_e} \quad (10)$$

The additional material parameters used here are the kinematic viscosity ν, the thermal diffusivity κ, the thermal expansion coefficient α, and gravity g_o at outer radius r_o.

Rigid conditions are used for the velocity at both boundaries. The inner core is electrically

conducting and rotates under the influence of Lorentz and viscous torques. An inner core dynamo equation and the inner core angular momentum budget are solved simultaneously with the system of Eqs. 1–5. The outer boundary is treated as an electrical insulator. Pseudospectral methods are employed with spherical harmonics up to degree 53 for the horizontal representation and Chebyshev polynomials up to degree 30 in radius. The equation system is time-stepped with a mixed implicit/explicit algorithm. For more details on the numerical model we refer to [6,9].

3. Results

3.1. Stability of axial and equatorial dynamos

Fig. 1 presents a sequence of computations for the parameter set $E=10^{-3}$, $Pr=1$, $q=14.3$, $\gamma=0.5$. We start with a Rayleigh number of $Ra=62$ and initialize a small magnetic seed field that contains an equatorial as well as an axial dipole component. The convective flow amplifies the equatorial field while the axial field decays. At $t=54.33$ the Rayleigh number is increased to $Ra=70$ (in red) and the dynamo changes to a reversing state that switches between normal and reversed axial dipole solutions. At $t=56$ the Rayleigh number is decreased back to $Ra=62$ (in blue). The dynamo remains dominated by an axial dipole but stops reversing. (The dependence of the reversal rate on the Rayleigh number is explored by Kutzner and Christensen [10].)

We can switch back to the equatorial solution by adding an equatorial dipole component to the axial magnetic field solution and restart the calculation with the so modified field (at $t=61$ in Fig. 1). Convection practically ceases and the system recovers to an equatorial dipole configuration. The added equatorial component has to be strong enough with an energy of at least 25% of the total magnetic energy.

These calculations demonstrate that stable equatorial as well as axial solutions can be found at identical parameters. The axial solution is subcritical at $Ra=62$ while the equatorial solution is supercritical. We have also started calculations with a seed field of axial and equatorial dipole components at $Ra=70$. Once more, only the equatorial contribution is amplified at first, but the equatorial solution is metastable. Lorentz forces change the flow field in a way that enables axial solutions to grow. These replace the equatorial solution after roughly one magnetic diffusion time. We therefore also regard the axial solution at $Ra=70$ as subcritical.

The differences that are responsible for the axial dipole contributions growing and destabilizing the equatorial ones are quite subtle and could not be pinned down. Kinematic dynamo calculations [2] have shown that minor changes in the flow can select very different eigenvectors. As we will show, the axial dynamo configuration is more compatible with the convective flow than the equatorial case. It thus seems likely that the stronger flows at higher Rayleigh numbers will destabilize the equatorial solution but will allow for the axial configuration.

Fig. 2 shows a stability diagram of axial and equatorial dynamo solutions in the Rayleigh number–radius ratio space for $E=10^{-3}$, $q=14.3$, and $Pr=1$. The solutions described above are included. Equatorial dipole solutions are stable and supercritical in the white shaded region but are metastable in the dark shaded region. All tested axial dynamo solutions are subcritical in the sense explained above.

Fig. 1 compares kinetic energies for the equatorial dynamo, the axial dynamo, and the convective solution at $Ra=62$. The kinetic energy in both dynamo configurations is only about 50% of the kinetic energy in the convective case. However, the energy associated with zonal flows (axial toroidal kinetic energy) amounts to only 0.5% of the total kinetic energy in the equatorial dynamo, while it is an order of magnitude larger in the axial dynamo and in the convective case. Moreover, the axial dynamo is much more efficient than the equatorial case, the ratios of magnetic to kinetic energies are $q_e=E_m/E_k\approx 65$ in the axial configuration and $q_e\approx 3$ for the equatorial case.

Fig. 3 compares the z-vorticity in an azimuthal cut at 5° below the equatorial plane for the convective solution (A), the equatorial dynamo (B), and the axial dynamo (C). Though the amplitudes

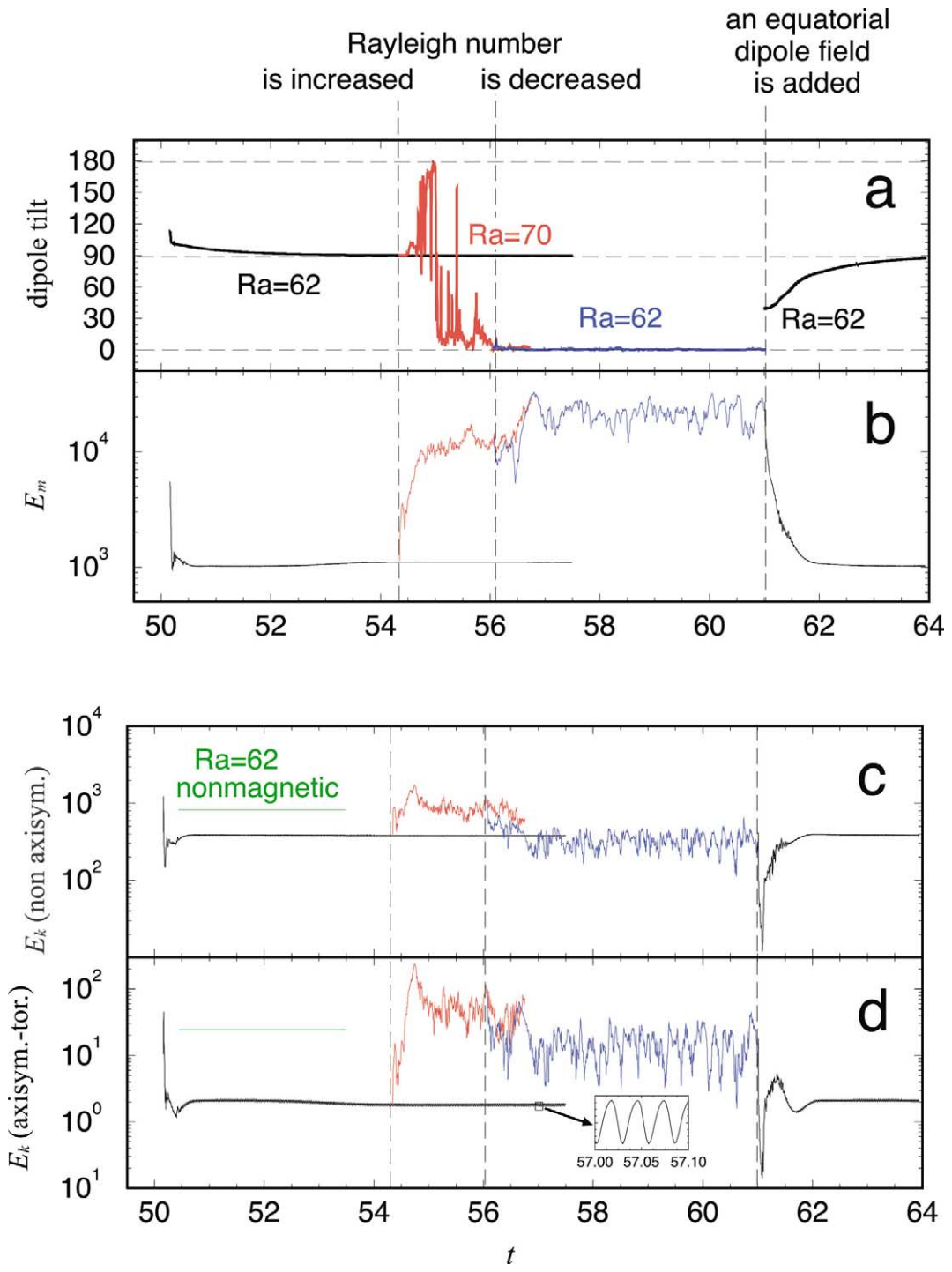

Fig. 1. (a) magnetic dipole tilt (degrees), (b) magnetic energy, (c) non-axisymmetric kinetic energy, and (d) axisymmetric toroidal (or zonal) kinetic energy for several runs at Rayleigh numbers $Ra = 62$ and $Ra = 70$. Other parameters are $\gamma = 0.5$, $E = 10^{-3}$, $Pr = 1$, and $q = 14.3$. Dynamo with equatorial and axial dipole geometry are both stable at $Ra = 62$.

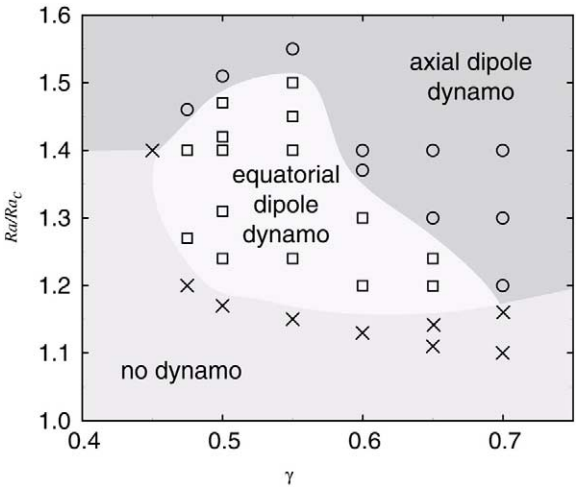

Fig. 2. Stability diagram for $E=10^{-3}$, $q=14.3$, $Pr=1$, varying radius ratio γ, and Ra/Ra_c, where Ra_c is the critical Rayleigh number for the onset of convection. Crosses mark failed dynamos, squares are parameter sets for which either axial or equatorial dynamos can be found, circles are parameter sets for which only the axial dynamos are stable.

differ, the vorticity pattern in the convective case and the equatorial dynamo are quite similar. Cyclones and anticyclones are of comparable size in both cases. The differences in relative zonal flow strength can probably by attributed to minor differences in the shape of the vortices that are responsible for differences in Reynolds stress. The axial dynamo solution, however, is dominated by anticylcones. We will see below that the cyclones are suppressed by magnetic back reaction in this case. The disparity between positive and negative vorticity accounts for a mean zonal flow that is about a factor 5 larger than in the equatorial dipole solution.

Note that the flow has an azimuthal symmetry of wave number $m=5$ in the axial dynamo solution but is of wave number $m=6$ in the purely convective and the equatorial dynamo cases. In addition, the equatorial cuts through the anticyclones have a more rounded shape in the axial dipole solution (see Fig. 3). Both properties account for less viscous diffusion. To some degree, this can also be translated to magnetic diffusion since the magnetic field is produced locally by the action of cyclones and anticyclones (see below). We speculate that the larger diffusion in the equatorial dynamo case is responsible for the fact that no solution of this type can be found beyond a radius ratio of $\gamma=0.7$ (Fig. 2).

Convective instabilities are of higher azimuthal wave number in the thinner shells at larger radius ratios. At $\gamma=0.7$ the convective flow is of $m=20$ for the equatorial dynamo solutions (which are ultimately unstable at this radius ratio), while it is $m=16$ with an axial dipole. Another reason why equatorial solutions cease to exist at larger radius ratios may simply be sought in the large disparity between the $m=1$ magnetic field and a high wave number convective field. The $m=1$ magnetic mode corresponds to a large scale cor-

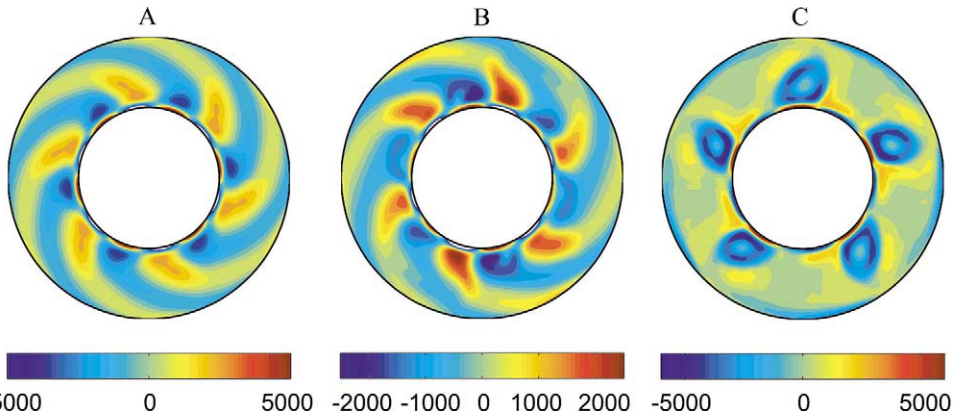

Fig. 3. Axial vorticity maps for (A) the non-magnetic convection case, (B) the equatorial dipole case at time $t=54.3$, and (C) the axial dipole case at time $t=56.6$.

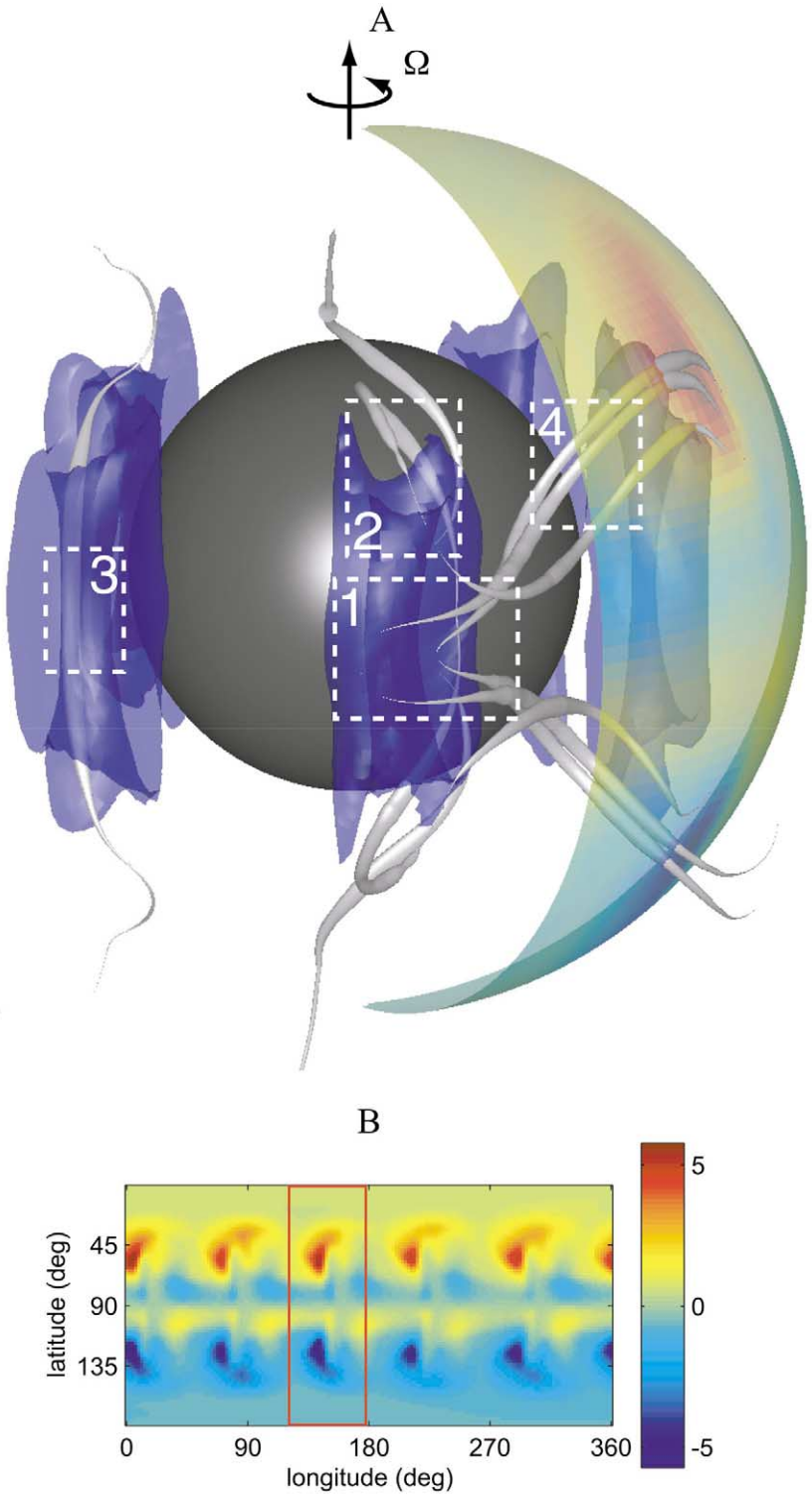
A
Ω
1
2
3
4
B
latitude (deg)
45
90
135
0
90
180
270
360
longitude (deg)
5
0
-5

relation in azimuth, which is not very likely considering the small scale flow background that feeds the magnetic field.

3.2. Nature of the axial dipole dynamo

The axial dipole dynamo is similar in nature and mechanism to the α^2 dynamos studied earlier [6]. We present a new visualization (Fig. 4) that highlights differences between the equatorial and axial dipole mechanisms and refer to [6] for a more detailed analysis. Fig. 4A shows anticyclones, selected magnetic field lines, and the inner core. Also shown is a section of the outer boundary with color-coded radial magnetic field, outward (inward) directed field in plotted in red (blue). Anticyclones are represented by blue isosurfaces of negative axial vorticity, cyclones have a much lower amplitude and are not shown here.

The rendered magnetic field lines illustrate the field–vortex interaction. Their thickness has been weighted with the magnetic pressure $\mathbf{B}^2$. This representation has several advantages. First, it allows to judge which lines are energetically important. Second, it gives an idea of the Lorentz forces acting perpendicular to the line. The Lorentz force can be interpreted as the sum of a magnetic tension and a magnetic pressure gradient:

$$(\nabla\times\mathbf{B})\times\mathbf{B} = \left[(\mathbf{B}\cdot\nabla)\mathbf{B} - \nabla\left(\frac{\mathbf{B}^2}{2}\right)\right]. \tag{11}$$

We switch to a local curvilinear coordinate system that is spanned by the tangential unit vector $\boldsymbol{e_s}$ along the field line, the normal unit vector $\boldsymbol{e_n}$ in the local field line plane, and the binormal vector $\boldsymbol{e_b} = \boldsymbol{e_s}\times\boldsymbol{e_n}$. Magnetic tension is then given by:

$$(\mathbf{B}\cdot\nabla)\mathbf{B} = \frac{\mathbf{B}^2}{R_c}\mathbf{e_n} + \frac{\partial}{\partial s}\left(\frac{\mathbf{B}^2}{2}\right)\mathbf{e}_s. \tag{12}$$

Here, R_c is the local curvature radius and s is the coordinate along $\boldsymbol{e_s}$. Plugging this into the Lorentz force expression Eq. 11 results in:

$$(\nabla\times\mathbf{B})\times\mathbf{B} = \left[\frac{\mathbf{B}^2}{R_c}\mathbf{e_n} - \nabla_H\left(\frac{\mathbf{B}^2}{2}\right)\right]. \tag{13}$$

with $\nabla_H = \nabla - \boldsymbol{e_s}\partial/\partial s$. The Lorentz force is thus strong where magnetic pressure and field line curvature are large. Moreover, magnetic pressure variations between adjacent lines carry information on the Lorentz force.

Fig. 4 indicates that the magnetic pressure inside the anticyclones (area 3) is larger than at their perimeter (areas 1 and 2). The respective magnetic pressure gradient is mainly balanced by the Coriolis force. The strong poloidal field lines sitting in the center of the antivortices are aligned with the vortex axis (area 3). Responsible for the alignment is a secondary flow directed away from the equator towards the northern and southern end of the vortex columns. This flow plays an important role in the poloidal field production [6]. Axially aligned field minimizes the flow disruption due to Lorentz forces.

The picture is different for the cyclones, where the internal secondary flow is directed equatorwards. It collects magnetic field near the outer boundary and stretches the field lines down the columnar axis (area 4). However, the field is also expelled from the vortex resulting in strong field lines that cross the vorticity structure (lower part of area 4). The associated Lorentz force brakes the vortex motion and is responsible for the dominance of anticyclones in the system, as observed in an earlier study [11]. Note that this selection of anticyclones is the result of a magnetic instability. Flow instabilities also tend to favor anticyclones but only at considerably higher Rayleigh numbers [12].

3.3. The equatorial dipole dynamo mechanism

Fig. 5 illustrates the field configuration in the equatorial dynamo solutions. The field is mainly symmetric with respect to the equator but also

←

Fig. 4. The axial dipolar dynamo at $t = 56.6$. (A) Axial vorticity isosurface (value -1400), and magnetic field lines. The line thickness is weighted by B^2. (B) Radial component of the magnetic field at the outer boundary (red is outwards). The zone within the red rectangle is represented on image A.

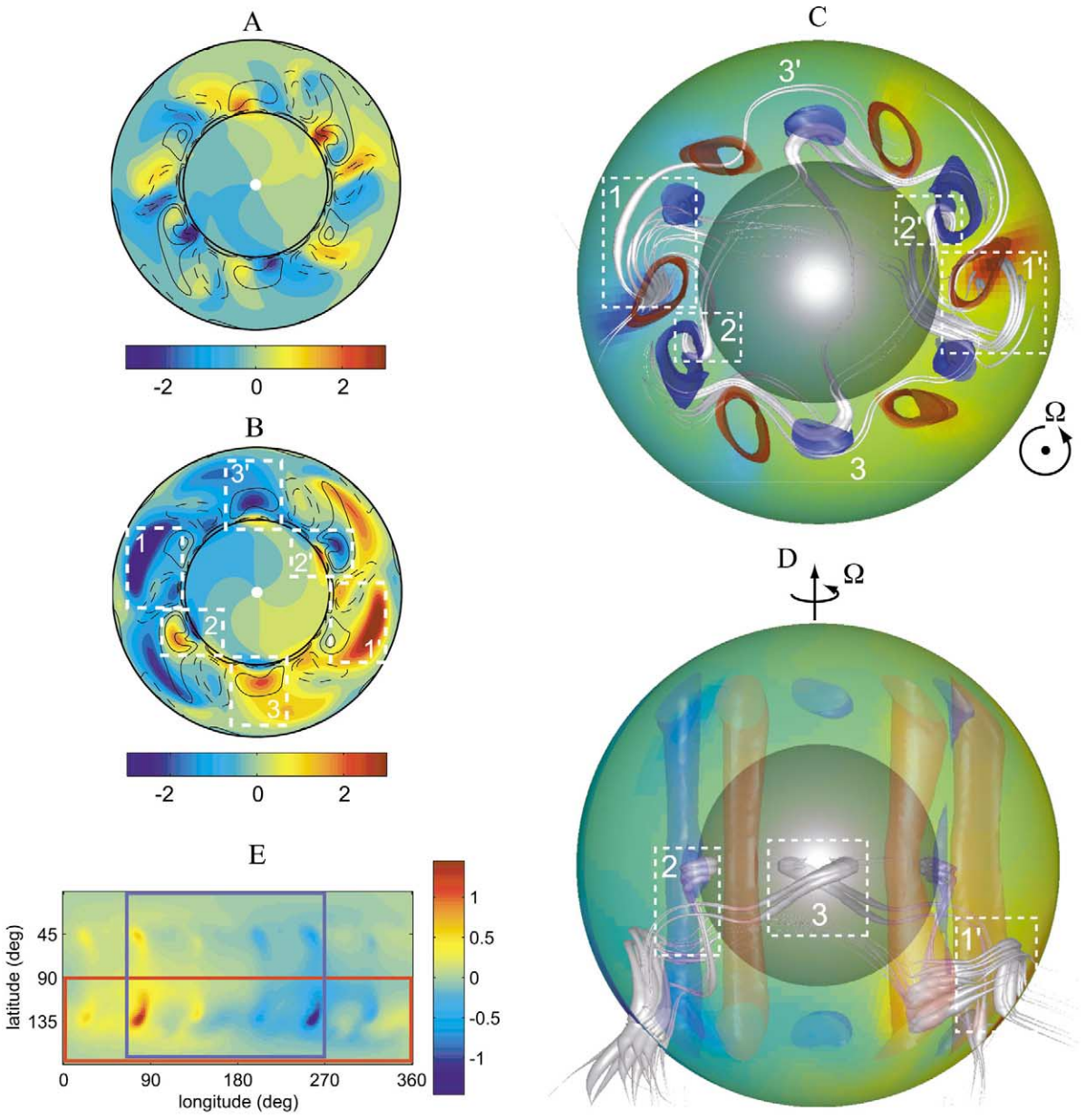

Fig. 5. Representations of the equatorial dipole dynamo at time $t = 54.3$. Color-coded radial (A) and azimuthal (B) magnetic field five degrees below the equatorial plane (see text), with contours of the axial vorticity (dashed lines are cyclones). (C,D) Magnetic field lines representations, from above and from the side. On the side view only the front half of vortices is represented for clarity. Flow and field lines in zones 1 and 1′, 2 and 2′, 3 and 3′ are identical, only the direction of the field changes, so each zone can be viewed from two angles. Isosurfaces −1400 (blue) and 1400 (red) of the axial vorticity are represented. (E) Same as in figure with axial plots (B). The outer boundary slices represented in (B) and (D) are respectively delineated in red and blue.

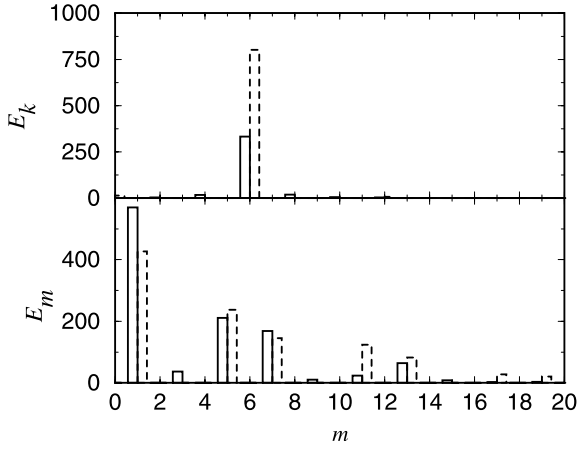

Fig. 6. Spectral decomposition of E_k and E_m with the azimuthal mode number m. Solid line is the self-sustained equatorial dynamo case. Dashed line is the kinematic dynamo case where the Lorentz force is turned off (convection structure is then identical to the non-magnetic case). E_m in the kinematic case is normalized to the value of E_m in the self-consistent case.

has a non-negligible antisymmetric component (see Fig. 5E). For simplicity we will neglect the latter in the following exploration.

Toroidal and poloidal magnetic energy are dominated by the $m=1$ contributions. However, the field is locally produced by the cyclones and anticyclones, the action of this $m=6$ flow on the large scale $m=1$ field results in a combination of $m=5$ and $m=7$ magnetic field contributions according to the non-linear selection rules in the dynamo equation. Fig. 6 shows the magnetic energy content in the respective wave number contributions.

The mechanism of poloidal field production is a typical α-process that is also working in the axial dynamo case. The differences in the resulting poloidal field structures are caused by the different toroidal field symmetries. This mechanism is commonly explained by the action of a cyclone/anticyclone pair on azimuthal toroidal field, we refer to [6] and their Fig. 5A. In the axial dipole case the opposite sign of the azimuthal toroidal field in the Northern and Southern Hemispheres results in production of a poloidal field that also changes its sign at the equatorial plane. In the equatorial dynamo, the azimuthal toroidal field is symmetric with respect to the equator and so is the poloidal radial field.

A key feature of the α-process is the wrapping of field lines around cyclones and anticyclones which can clearly be identified in Fig. 5C. The radial magnetic field thus changes its sign in azimuthal direction within each cyclone and each anticyclone (Fig. 5A). The secondary flow described above concentrates magnetic field in the equatorial region of anticyclones (Fig. 5A and zones 3 and 3′ in Fig. 5C) and where cyclones touch the outer boundary (Fig. 5D,E).

The mechanism of toroidal field production can be categorized as an α-mechanism since the toroidal field is locally produced by the action of cyclones and anticyclones. The process suggested by [6] is only part of the answer here. It is mainly working in regions where the meridional component of the poloidal field is significant. Azimuthal toroidal field is mainly produced where the radial poloidal field is strong (see for example regions 1 and 1′ in Fig. 5C,D). The respective mechanism is shearing of radial field by radial gradients in the azimuthal flow. Especially apparent is this effect where strong radial magnetic field leaves and enters the outer boundary, these regions are labeled 1 and 1′ in Fig. 5. Note that the field lines are also very thick, i.e. energetic, in these regions. The local effects of azimuthal toroidal field production are correlated in a way that guarantees production of a large scale $m=1$ component. Two separate radial layers can be distinguished with a phase difference of one cyclone/anticyclone pair in the azimuthal field component. (Fig. 5B,C).

Since the toroidal field loops close within the Northern and Southern Hemispheres latitudinal field components are as important as the azimuthal components. The latitudinal toroidal field is produced by the shearing of azimuthal poloidal field between the secondary poleward flows in anticyclones and equatorward flows in cyclones. There are two regions where this effect is dominating the production of azimuthal toroidal field, these are also the regions where the azimuthal toroidal field changes sign (regions 2 and 2′ in Fig. 5C,D).

The orientation of the poloidal magnetic field along the axis of anticyclones in the axial dipole

case plays no important role in the equatorial dipole solutions. Here, magnetic field passes horizontally through cyclones and anticyclones. Both are braked by the associated Lorentz forces. This effect is stronger in anticyclones because of the increased field strength at the equatorial plane (see above). Consequently, the amplitude of the anticyclonic columns is somewhat smaller than that of the cyclones.

This also suggests an answer to the question of why the axial dipole is so much more efficient than the equatorial case. In the axial dipole dynamo, most of the kinetic energy is carried by anticyclones and these are also more active elements in poloidal field production. The axial orientation of poloidal magnetic field in these columns minimizes the interaction with the flow. In the equatorial dipole dynamo the magnetic field lines impair the motion of cyclones as well as anticyclones. This requires a much lower equilibrium field strength than in the axial case. An increase in magnetic field amplitude would brake cyclones as well as anticyclones, it would therefore reduce the magnetic field production, and it would ultimately cause the field strength to decrease again.

The fact that the convective flow is less disrupted by magnetic field lines in the axial dipole case also means that this configuration can accommodate stronger convective flows. As stated above, this is probably the reason why only axial dipole dynamos remain stable at higher Rayleigh numbers.

A few words about the time dependence of the equatorial dipole solution. The magnetic energy is almost steady in the equatorial dipole dynamo (Fig. 1d). But magnetic field and velocity field drift as prograde-propagating waves with periods reported in Table 1. To check the influences of magnetic back reaction on the flow we have also performed a calculation without the Lorentz force in the Navier–Stokes Eq. 1. The resulting magnetic field is very similar to the solution of the full problem which indicates that the equatorial dynamo is close to being kinematic. However, there are some differences in the time behavior. The drift period of the $m=5$ and $m=7$ magnetic field components is determined by the drift of the $m=6$ convective instability. The much slower drift of the $m=1$ dipole component, on the other hand, is determined by the magnetic instability and seems to be independent of the convective drift. Respective periods differ significantly between the kinematic (no Lorentz force) and the full problem.

There is also an additional fast oscillation of low amplitude in the convective as well as in the magnetic field (see inset in Fig. 1). This oscillation is a result of the relative drift of the $m=6$ flow structure with respect to the $m=1$ magnetic field, the convective columns 'feel' variations in the Lorentz force. The oscillation is in turn translated to the magnetic field via small variations in the local dynamo mechanism. Consequently, these oscillations are missing when we switch out the magnetic back reaction on the flow.

Table 1
Drift periods for the main components of the dynamo, the flow component and the energetic oscillation

	Kinematic	Self-consistent
$m=1$	2.98 ± 0.4	0.682
$m=5$	0.124	0.116
$m=6$ (flow)	0.148	0.135
$m=7$	0.171	0.152
Oscillation	none	0.023

4. Implications for planetary dynamos

We have demonstrated that the magnetic field strength saturates at a much lower level in the equatorial dipole configurations than in the axial dipole cases. The Elsasser number $\Lambda = \sigma B^2/\rho\Omega$ (σ is the fluid conductivity) measures the relative importance of Lorentz and Coriolis forces in the Navier–Stokes Eq. 1. It can also be interpreted as a measure for the relative magnetic field strength. The ratio of the Elsasser number Λ_a of the axial dynamo and the Elsasser Λ_e number of the equatorial dynamo that have been examined above ($Ra=62$) is $\Lambda_a/\Lambda_e = 20$.

What is this ratio for planetary dynamos? Planetary magnetic fields that are dominated by axial dipoles have Elsasser numbers of order one (Earth, Jupiter, Saturn). The internal models of Uranus and Neptune are not very well con-

strained yet. For example, it is still unknown where the dynamo region is located. The surface fields of Uranus and Neptune are about as large as the geomagnetic surface field, we simply assume here the fields in the dynamo region are also of comparable magnitude. The electrical conductance in the interior of Uranus and Neptune is most likely carried by water and ammonia ions. Ab-initio calculations suggest conductivities of the order 10^4 S/m [13]. These estimates give an Elsasser number of order 10^{-2}. We thus arrive at a ratio Λ_a/Λ_e of order 10^2 for the planetary dynamos in our solar system.

The dynamo models explored here suggest that the lower field strength in the equatorial dipole configurations is a consequence of the mainly transverse field lines that oppose the shearing motion of axial vorticity columns. This can possibly by generalized to all dynamos in rapidly rotating systems whose dipole axis is significantly tilted away from the rotation axis. We therefore propose that the anticipated lower Elsasser numbers for Uranus and Neptune are likely and that this fact is strongly related to the inclination of the magnetic dipole axes.

Acknowledgements

J.A. acknowledges support through a European Community Marie Curie Fellowship under contract number HPMF-CT-2001-01364 during the research phase of this work. J.W. has been supported by the German Science Foundation within the Scientific Priority Program 'Geomagnetic Variations'. The authors thank Peter Olson and an anonymous referee for comments which substantially improved this study.*[VC]*

References

[1] R. Holme, J. Bloxham, The magnetic field of Uranus and Neptune: Methods and models, J. Geophys. Res. 101 (1996) 2177–2200.
[2] D. Gubbins, C.N. Barber, S. Gibbons, J.J. Love, Kinematic dynamo action in a sphere, II. Symmetry selection, Proc. R. Soc. Lond. A 456 (2000) 1669–1683.
[3] R. Stieglitz, U. Müller, Experimental demonstration of the homogeneous two-scale dynamo, Phys. Fluids 1 (2001) 561–564.
[4] G.A. Glatzmaier, P.H. Roberts, A three dimensional self consistent computer simulation of the geomagnetic field reversal, Nature 377 (1995) 203–209.
[5] W. Kuang, J. Bloxham, An Earth-like numerical dynamo model, Nature 389 (1997) 371–374.
[6] P. Olson, U. Christensen, G.A. Glatzmaier, Numerical modelling of the geodynamo: Mechanisms of field generation and equilibration, J. Geophys. Res. 104 (1999) 10383–10404.
[7] N. Ishihara, S. Kida, Equatorial magnetic dipole field intensification by convection vortices in a rotating spherical shell, Fluid Dyn. Res. 31 (2002) 253–274.
[8] E. Grote, F.H. Busse, A. Tilgner, Convection-driven quadrupolar dynamos in rotating spherical shells, Phys. Rev. E 60 (1999) R5025–R5028.
[9] J. Wicht, Inner-core conductivity in numerical dynamo simulations, Phys. Earth Planet. Int. 132 (2002) 281–302.
[10] C. Kutzner, U. Christensen, From stable dipolar to reversing numerical dynamos, Phys. Earth Planet. Int. 131 (2002) 29–45.
[11] A. Kageyama, T. Sato, Velocity and magnetic field structures in a magnetohydrodynamic dynamo, Phys. Plasmas 4 (1997) 1569–1575.
[12] J. Aubert, N. Gillet, P. Cardin, Quasigeostrophic models of convection in rotating spherical shells, Geophys. Geochem. Geosyst. 4, doi: 10.1029/2002GC000456.
[13] C. Cavazzoni, G.L. Chiarotti, S. Scandolo, E. Tosatti, N. Bernasconi, N. Parrinello, Superionic and metallic states of water and ammonia at giant planet conditions, Science 283 (1999) 44–46.